JOURNAL OF SOLID STATE CHEMISTRY 84, 39–51 (1990)

Crystallographic Distortion and Magnetic Structure of Terbium Iron Garnet at Low Temperatures

RAINER HOCK

Institut für Kristallographie der Universität, 6000 Frankfurt, Federal Republic of Germany; and Institut Laue-Langevin, F-38042 Grenoble, France

HARTMUT FUESS

Institut für Kristallographie der Universität, D-6000 Frankfurt, Federal Republic of Germany

THOMAS VOGT

Institut Laue-Langevin, F-38042 Grenoble, France

AND MICHEL BONNET

DRF/SPh-MDN, Centre d'Etudes Nucléaires de Grenoble, F-38041 Grenoble, France

Received April 26, 1989; in revised form August 14, 1989

The crystallographic and magnetic structures of terbium iron garnet were refined simultaneously from neutron powder patterns at four temperatures, 290, 39, 13, and 5 K, by the Rietveld method. The distortion from the cubic room-temperature structure (space group $Ia3d$, a = 12.4339(1) Å) leads to rhombohedral symmetry. $R\bar{3}$ is compatible with both the crystallographic and magnetic structure at low temperatures. The lattice constants are a_{rh} = 10.7442(1) Å and α = 109.412(1)° at 5 K. Precise values for the shifts of atomic parameters were derived and the evolution of the magnetic structure at low temperatures is given. No deviation from the collinearity has been observed for the iron spin sublattices. The results are compared with previous work.

Introduction

The rare earth iron garnets of general formula $\{Re_3\}(Fe_2)[Fe_3]O_{12}$ with Re = Tb, Dy, Ho, Er, . . . are isomorphous to natural garnets. At room temperature the garnets are cubic with space group $Ia3d$ (*1*). The atoms are located at positions 16*a* and 24*d* for octahedral and tetrahedral Fe^{3+}, respectively, 24*c* for the Tb^{3+} in dodecahedral coordination; O^{2-} ions occupy the general position 96*h*. Terbium iron garnet (TbIG) is one of the most thoroughly studied compounds in these series.

At room temperature TbIG is a classical example of Néel ferrimagnetism (T_c = 550

0022-4596/90 $3.00

K). The magnetic structure is a collinear spin arrangement of two antiferromagnetically coupled Fe sublattices, whereas the rare earth moments are aligned antiparallel to the resulting Fe^{3+} net moment (*1*, *2*). Below 130 K a noncollinear spin structure of the Tb^{3+} moments on two magnetically nonequivalent sites is reported (*3*, *4*). The terbium spins form a double cone around the [111] axis. The magnetic space group has been determined previously by powder neutron diffraction to be $R\bar{3}c'$ and the evolution of the Tb^{3+} moments as a function of temperature was studied in the range 550 to 4.2 K (*3*). A rhombohedral distortion of the cubic unit cell was observed related to the appearance of the noncollinear spin structure (*5–7*). The rhombohedral angle was measured as a function of temperature by Sayetat *et al.* by X-ray powder diffraction (*7*). These authors followed the splitting of the reflections {10 4 0} and {8 6 4} from the cubic to the rhombohedral symmetry. TbIG exhibits the most important magnetostriction of all rare earth iron garnets. This may be directly related to the highly anisotropic properties of the Tb^{3+} ions with respect to their exchange and crystal field interactions (*7*). Despite all these careful investigations, up to now no simultaneous determination of the complete low-temperature crystal and magnetic structure has been reported. Such an investigation should yield the atomic coordinates in the rhombohedral space group. The data may constitute a base for a further interpretation of the microscopic origins of magnetostriction in this compound (*7*). Powder diffraction was applied because single-crystal measurements on high-quality rare earth iron garnets suffer from severe extinction (*8–10*). Since high-resolution powder diffractometers like D2B at the ILL in Grenoble came into operation, detailed information about the distortions of ReIG's can be obtained from powder diffraction data (*11*).

Experimental and Data Reduction

Powder patterns of sintered polycrystalline TbIG were recorded on the powder diffractometer D2B at the ILL in Grenoble at 290, 39, 13, and 5 K. The sample was held in a vanadium can of 10 mm diameter and mounted in a helium bath cryostat. The diffractometer is equipped with a focusing Ge monochromator and a takeoff angle of 135°. A wavelength of $\lambda = 1.594$ Å from Ge {533} was used. The choice of this reflection excludes a $\lambda/2$ contamination. Each pattern was taken up to $2\theta = 150°$ in steps of 0.025° in 4 hr. At room temperature this corresponds to a recorded d-spacing interval of $0.83 < d < 5.07$ Å. At 5 K the existence of additional pure magnetic Bragg reflections extends this interval to $0.83 < d < 8.79$ Å. All powder patterns were analyzed by the Rietveld refinement method (*11*). Lorentz correction was applied. Up to $2\theta = 50°$ we accounted for an asymmetric peak shape due to finite detector height by an asymmetry parameter according to the formalism given by Rietveld (*12*). The background was determined at 48 positions and substracted after a linear interpolation. Magnetic form factors for Fe^{3+} were from (*13*) and those for Tb^{3+} from (*14*). The scattering lengths for iron and oxygen were from Sears (*15*); for Tb the value redetermined on TbIG and TbO_2 by Fuess *et al.* (*16*) was used ($b = 7.38$ fm). In the room-temperature pattern the region between 84.75° and 88.78° in 2θ was excluded from the refinement. It was accidentally masked by a cryostat tube covering partially this 2θ range.

The magnetic matrices describing the symmetry of the spin configuration were calculated with a program developed by one of us (M. Bonnet). The program applies the macroscopic method of Bertaut (*17*) based on group theoretical arguments. In all previous investigations of the magnetic structure of TbIG, the nuclear contribution

to the scattered intensity was determined separately from data above the Curie point (T_c = 550 K) and then substracted from the total scattering at low temperatures. This is a source of uncertainty in the determination of the magnetic structure. The thermal motion as well as the positions of the individual atoms change between 550 and 4.2 K, yielding a different nuclear contribution to the total scattering especially in the rhombohedrally distorted phase.

Results

Crystal Structure of TbIG

The analysis of the powder pattern recorded at 290 K (Fig. 1) confirms the cubic structure of TbIG at elevated temperatures. All 88 unique reflections (total number of overlapping reflections is 152) up to 2θ = 148.5° could be indexed in space group *Ia*3*d*. Only two small impurity lines were found and excluded from the refinement. The results of our refinement of the magnetic and the nuclear structure are given in Table I. The refined magnetic moments are compared to previous work. The crystal structure agrees well with former structure determinations (*2*, *7*, *16*, *18*). We adopted the Néel model of a uniaxial ferrimagnetic spin configuration along the [111] axis to describe the magnetic structure (*1*). The reduced magnetic moments of the Fe^{3+} ions of 3.37 and 3.70 μ_B compared to the expected free ion value at 300 K of 4.3 μ_B (*16*) are a common result in magnetic structure refinements of garnets and other oxides as well as fluorides. The latter ones may show additional topological frustration (*19*).

Crystal Structure at 5 K

Figure 2 shows the powder pattern of TbIG at 5 K. Clearly additional purely magnetic lines appear due to the deviation of

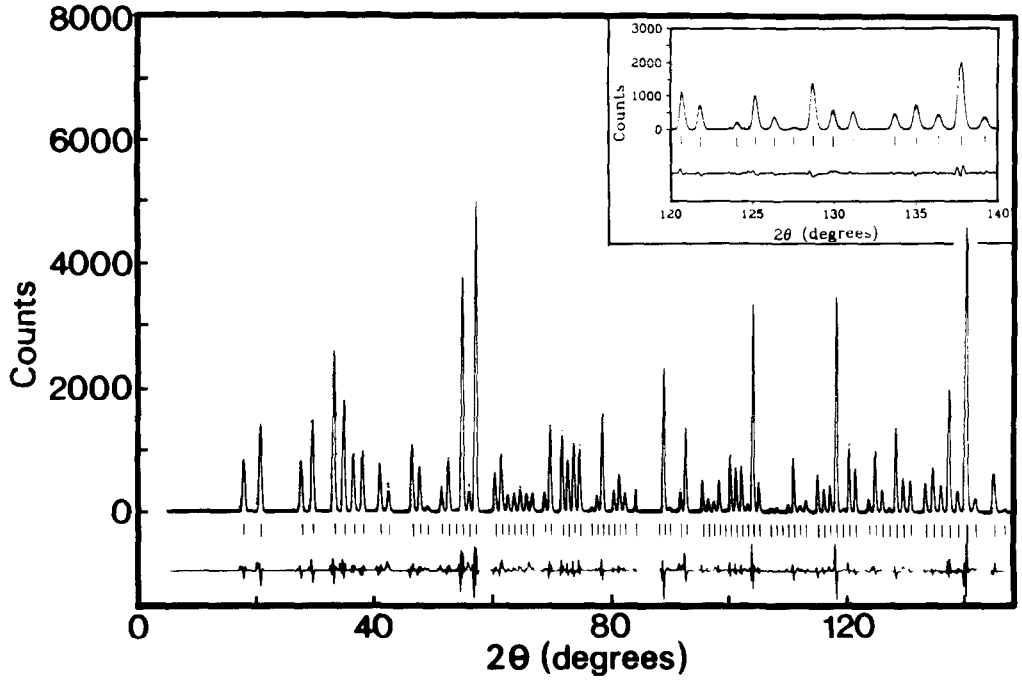

FIG. 1. Neutron diffraction pattern of TbIG at room temperature (T = 290 K).

TABLE I

MAGNETIC MOMENTS AND POSITIONAL PARAMETERS AT 290 K IN TbIG

	Ia3d							
Ref.	Fe16*a* $\lvert m_a \rvert$ (μ_B)	Fe24*d* $\lvert m_d \rvert$ (μ_B)	Tb24*d* $\lvert m_c \rvert \cdot$ (μ_B)		$(\sin\theta/\lambda)_{max}$	$\lvert M_{bulk} \rvert$ (μ_B mole^{-1})		$R_{mag.}$
(*3*)	4.32	4.19	1.16		0.28	0.9		
(*16*)	3.69(10)	3.65(10)	1.15(9)		0.53	0.24		
(*2*)	4.66	4.24	1.04		0.30	0.56		
This work	3.70(5)	3.37(5)	1.12(5)		0.61	1.3		0.067
Atomic positions and unit cell								
a_c(Å)	*X*	*Y*	*Z*	B_a^{Fe}	B_d^{Fe}	B_c^{Tb}	B_h^{oxy}	$R_{Nuc.}$
12.4339(1)	−0.02752(9)	0.05570(11)	0.15018(10)	0.405(18)	0.375(19)	0.392(15)	0.492(26)	0.044

the Tb^{3+} moments from collinearity. A splitting of most of the reflections due to the rhombohedral cell distortion is observed above $2\theta = 70°$ (see inset in Figs. 1 and 2).

The crystal structure of TbIG at 5 K was refined in space group $R\bar{3}$. Table II displays the splitting of the four atomic sites in space group *Ia3d* into 18 sites in $R\bar{3}$. In this space group the general position 96*h* of *Ia3d* for oxygen splits into eight general positions 6*f* (*1–8*), with 24 oxygen parameters. The 24*d* tetrahedral iron sites and the 24*c* dodecahedral terbium sites become general positions 6*f* as well. Only the 16*a* octahedral iron site

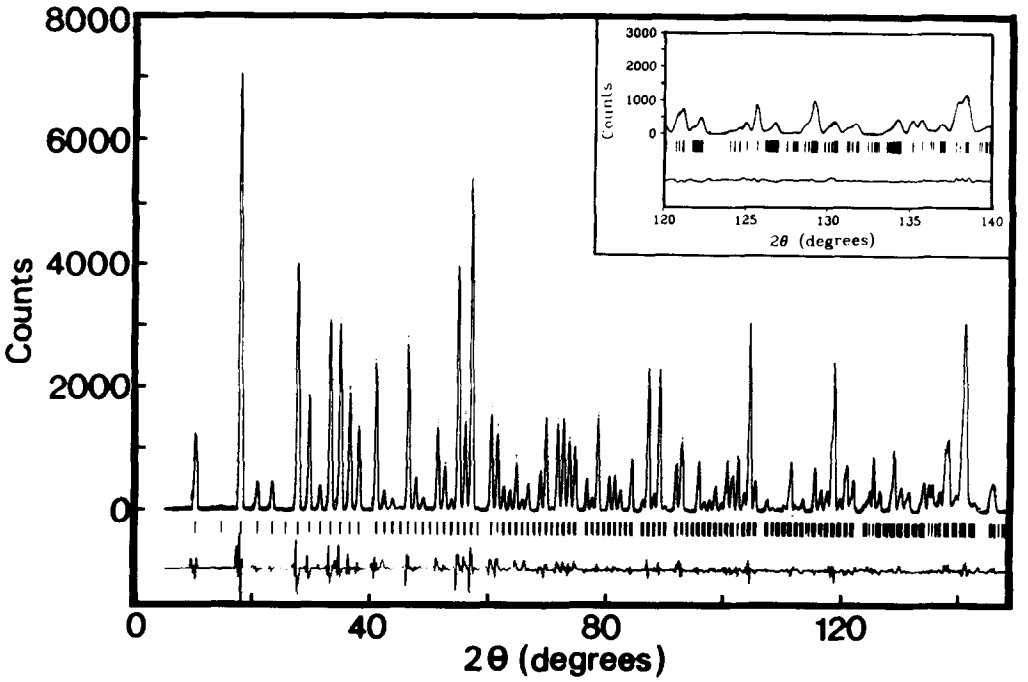

FIG. 2. Neutron diffraction pattern of TbIG at $T = 5$ K in the rhombohedral distorted phase.

TABLE II

RELATION OF ATOMIC POSITIONS IN *Ia*3*d* AND $R\bar{3}$

	Space group					
	$Ia3d$-(O_h^{10})			$R\bar{3}$-(C_{3i}^2)		
Atom	Site	Symmetry	Position	Site	Symmetry	Position
Tb^{3+}	24*c*	222	$\pm(\frac{1}{8}0\frac{1}{4})$ c.p.	6*f*	1	$\pm(xyz) \triangleq (\frac{3}{8}\frac{1}{8}\frac{1}{4})$
			$\pm(\frac{3}{8}0\frac{3}{4})$ c.p.	6*f*	1	$\pm(xyz) \cong (\frac{7}{8}\frac{5}{8}\frac{1}{4})^a$
Fe^{3+}	24*d*	$\bar{4}$	$\pm(\frac{3}{8}0\frac{1}{4})$ c.p.	6*f*	1	$\pm(xyz) \cong (\frac{5}{8}\frac{3}{8}\frac{1}{4})$
			$\pm(\frac{1}{8}0\frac{3}{4})$ c.p.	6*f*	1	$\pm(xyz) \simeq (\frac{7}{8}\frac{1}{8}\frac{3}{4})^a$
Fe^{3+}	16*a*	$\bar{3}$	(000), $(\frac{1}{4}\frac{1}{4}\frac{1}{4})$,	1*a*	$\bar{3}$	(000)
			$(0\frac{1}{2}\frac{1}{2})$ c.p.	1*b*	$\bar{3}$	$(\frac{1}{2}\frac{1}{2}\frac{1}{2})$
			$(\frac{1}{4}\frac{3}{4}\frac{3}{4})$ c.p.	3*e*	$\bar{1}$	$(0\frac{1}{2}\frac{1}{2})$ c.p.
				3*d*	$\bar{1}$	$(\frac{1}{2}00)$ c.p.
O^{2-}	96*h*	1	$(xyz)^b$	6*f*	1	(xyz) $O_{I\text{-}VIII}{}^a$

Note. c.p., cyclic permutation.

[a] For refined positions, see Table III.

[b] For refined positions, see Table I.

splits into four (1*a*, 1*b*, 3*e*, and 3*d*) special positions.

We refined four isotropic thermal parameters, corresponding to the atom sites in space group *Ia*3*d*. Attempts to refine individual isotropic or even anisotropic temperature factors produced unreasonable results. The refined values were in fact in some cases as big as their standard deviations and the deviation among individual factors for oxygens was rather important. The reasons are (i) the deviation of atomic positions from the ideal cubic position is only small, and (ii) the correlation between temperature factors is important. We think that even extremely good powder data can not produce reliable individual temperature factors under similar conditions.

The refinement includes a total of 56 parameters with a set of 531 unique reflections (total number of overlapping reflections is 1170 in $R\bar{3}$) up to $2\theta = 148.5°$. The lattice constants of the rhombohedral cell and the atomic coordination are compared to the starting values at room temperature transformed to the rhombohedral cell (Table III). The values of the lattice constants a_0 and α_0 are in good agreement with the work of Sayetat (*5*) (see Table III).

Magnetic Structure at 5 K

The most recent refinement of the magnetic structure from a powder pattern was performed by Lahoubi *et al.* (*3*). They reported the magnetic moments on two distinct Tb^{3+} sites 6*e* and 6*e*′ in space group $R\bar{3}c'$ as a function of temperature. As reflections of the type {200}, {600}, {422} were not observed, the authors deduced the magnetic space group to be $R\bar{3}c'$. The absence of {200}, {600}, {422} indicates components of the Tb moments perpendicular to the [111] axis of equal magnitude and opposite sign $m^{\perp}(\text{Tb1}) = m^{\perp}(\text{Tb2})$, implying a glide plane *c*′ and thus the magnetic space group $R\bar{3}c'$.

In contrast to their findings we observe in our pattern the reflections {200}, {600}, {422}. (The reflections are given in cubic notation (Fig. 3)). Close inspection of the experimental data explains why these reflections were not observed before. The ratio of

TABLE III

ATOMIC PARAMETERS OF THE CRYSTAL STRUCTURE AT 5, 13, 39, AND 290 K

		$R\bar{3}$			
		Temperature: 290 K		R = 0.044	
Atoms		X	Y	Z	B
Fe(oct)	(1)	0.0000	0.0000	0.0000	0.42(2)
	(2)	0.5000	0.5000	0.5000	0.42(2)
	(3)	0.0000	0.5000	0.5000	0.42(2)
	(4)	0.5000	0.0000	0.0000	0.42(2)
Fe(tet)	(1)	0.6250	0.3750	0.2500	0.36(2)
	(2)	0.8750	0.1250	0.7500	0.36(2)
O	(1)	0.2060(1)	0.1227(1)	0.0282(1)	0.50(1)
	(2)	0.5832(1)	0.1777(1)	0.2060(1)	0.50(1)
	(3)	0.1227(1)	0.5945(1)	0.9168(1)	0.50(1)
	(4)	0.9055(1)	0.0282(1)	0.3223(1)	0.50(1)
	(5)	0.3773(1)	0.2941(1)	0.4718(1)	0.50(1)
	(6)	0.3223(1)	−0.0832(1)	0.2971(1)	0.50(1)
	(7)	−0.0945(1)	0.3773(1)	−0.4168(1)	0.50(1)
	(8)	0.4718(1)	−0.4055(1)	0.1777(1)	0.50(1)
Tb	(1)	0.3750	0.1250	0.2500	0.40(2)
	(2)	0.8750	0.6250	0.2500	0.40(2)
a_c = 12.4339(1) Å a_{rh} = 10.7679(1) Å α = 109.47°					
		Temperature: 39 K		R = 0.039	
Atoms		X	Y	Z	B
Fe(oct)	(1)	0.000	0.000	0.000	0.22(2)
	(2)	0.500	0.500	0.500	0.22(2)
	(3)	0.000	0.500	0.500	0.22(2)
	(4)	0.500	0.000	0.000	0.22(2)
Fe(tet)	(1)	0.626(1)	0.373(1)	0.251(1)	0.21(2)
	(2)	0.877(1)	0.125(1)	0.753(1)	0.21(2)
O	(1)	0.213(2)	0.128(2)	0.030(2)	0.36(2)
	(2)	0.586(2)	0.176(2)	0.209(2)	0.36(2)
	(3)	0.115(2)	0.587(2)	0.912(2)	0.36(2)
	(4)	0.908(2)	0.038(2)	0.325(2)	0.36(2)
	(5)	0.384(2)	0.305(2)	0.483(1)	0.36(2)
	(6)	0.318(2)	−0.082(2)	0.294(1)	0.36(2)
	(7)	−0.096(2)	0.375(1)	−0.421(2)	0.36(2)
	(8)	0.473(2)	−0.413(2)	0.176(2)	0.36(2)
Tb	(1)	0.376(1)	0.126(1)	0.257(1)	0.11(2)
	(2)	0.871(1)	0.624(1)	0.249(1)	0.11(2)
a_{rh} = 10.7478(1) Å α = 109.432(1)°					

TABLE III—*Continued*

Atoms		Temperature: 13 K X	Y	Z	R = 0.039 B
Fe(oct)	(1)	0.000	0.000	0.000	0.20(2)
	(2)	0.500	0.500	0.500	0.20(2)
	(3)	0.000	0.500	0.500	0.20(2)
	(4)	0.500	0.000	0.000	0.20(2)
Fe(tet)	(1)	0.625(1)	0.372(1)	0.250(1)	0.27(3)
	(2)	0.878(1)	0.128(1)	0.753(1)	0.27(3)
O	(1)	0.211(2)	0.125(2)	0.032(2)	0.35(2)
	(2)	0.585(2)	0.174(2)	0.210(1)	0.35(2)
	(3)	0.115(1)	0.589(2)	0.911(1)	0.35(2)
	(4)	0.907(2)	0.033(2)	0.325(2)	0.35(2)
	(5)	0.379(2)	0.302(2)	0.482(2)	0.35(2)
	(6)	0.320(1)	−0.083(2)	0.296(1)	0.35(2)
	(7)	−0.096(2)	0.374(1)	−0.418(1)	0.35(2)
	(8)	0.472(2)	−0.412(2)	0.178(2)	0.35(2)
Tb	(1)	0.378(1)	0.125(1)	0.256(1)	0.06(2)
	(2)	0.871(1)	0.624(1)	0.252(1)	0.06(2)
		a_{rh} = 10.7444(1) Å	α = 109.413(1)°		
Atoms		Temperature: 5 K X	Y	Z	R = 0.038 B
Fe(oct)	(1)	0.000	0.000	0.000	0.23(2)
	(2)	0.500	0.500	0.500	0.23(2)
	(3)	0.000	0.500	0.500	0.23(2)
	(4)	0.500	0.000	0.000	0.23(2)
Fe(tet)	(1)	0.629(1)	0.374(1)	0.250(1)	0.30(3)
	(2)	0.876(1)	0.123(1)	0.752(1)	0.30(3)
O	(1)	0.208(1)	0.126(1)	0.033(1)	0.37(2)
	(2)	0.586(2)	0.179(2)	0.214(2)	0.37(2)
	(3)	0.118(1)	0.586(2)	0.911(2)	0.37(2)
	(4)	0.907(2)	0.034(2)	0.325(2)	0.37(2)
	(5)	0.381(1)	0.300(1)	0.482(1)	0.37(2)
	(6)	0.321(2)	−0.082(2)	0.299(2)	0.37(2)
	(7)	−0.099(2)	0.376(1)	−0.420(2)	0.37(2)
	(8)	0.472(2)	−0.412(2)	0.177(2)	0.37(2)
Tb	(1)	0.380(1)	0.127(1)	0.256(1)	0.03(2)
	(2)	0.870(1)	0.624(1)	0.253(1)	0.03(2)
		a_{rh} = 10.7442(1) Å	α = 109.412(1)°		

peak to background normalized to the intensity of the {110} reflection is 276 : 1 for Figs. 1 and 2, whereas it is 8 : 1 for previous measurements. It seems likely therefore that those reflections were not resolved from the background in previous patterns. Thus a comparison between them gives clear evidence on the improvements made in neutron powder diffraction. The observation of {200}, {600}, {422} leads us to describe the magnetic structure in $R\bar{3}$. In this space group the components of the Tb^{3+}

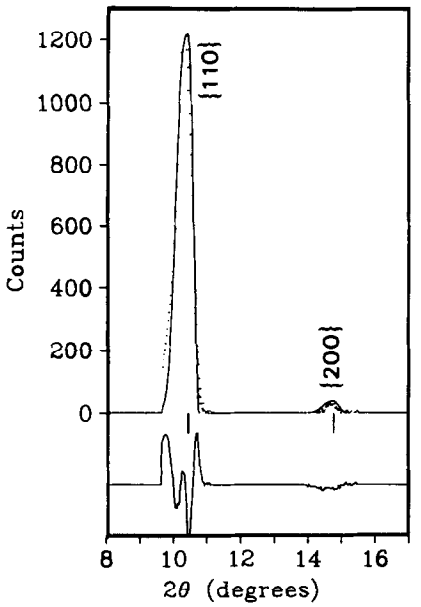

FIG. 3. Low-angle part of the diffraction pattern at 5 K. Shown are the first two pure magnetic reflexions {110} and {200} in cubic notation.

moments perpendicular to the unique threefold axis are no longer restricted to a plane and to equal magnitude. The constraint $m^{\perp}(\text{Tb1}) = m^{\perp}(\text{Tb2})$ is dropped.

The results of the refinement in space group $R\bar{3}$ are given in Table IV together with the results of Lahoubi at 4.2 K. The Tb moments at 5 K are close to the values previously reported (*3*). The refined angles of the moments with the unique threefold axis differ significantly from former results. The choosen [111], [$\bar{1}$10], [$\bar{1}\bar{1}$2] coordinate system together with the refined terbium spins m(Tb1) and m(Tb2) at 5 K is shown in Fig. 4.

The directions of the spins in Table IV are expressed in polar coordinates θ and Φ. These angles are defined in the coordinate system in Fig. 4. The inclination angle of the spins with the [111] axis is θ and Φ is the angle between the [$\bar{1}$10] axis and the spin components perpendicular to [111].

In Figs. 5a and 5b we visualize the difference in the two magnetic models $R\bar{3}c'$ and $R\bar{3}$. Again the [111], [$\bar{1}$10], [$\bar{1}\bar{1}$2] coordinate system is displayed together with six Tb spins, each trio of them corresponding to sites 6*f* and 6*f'*, respectively, related by 120 and 240° rotations, viewed down the [111] axis. Six other Tb spins of the unit cell related by the center of inversion are not shown.

TABLE IV

MAGNETIC STRUCTURE DETERMINATION AT 5, 13, AND 39 K COMPARED TO REF. (*3*)

T(K)	Site	m_x	m_y	m_z	$\lvert m\rvert$	$\theta_{1,2}$	$\Phi_{1,2}$	$R_{\text{mag.}}$
4.2 (*3*)	6*e*	7.48	2.35	2.35	8.18(0.02)	30.8(0.02)	90.0	0.060
5	$R\bar{3}c'$	9.38(0.1)	8.53(0.2)	5.71(0.1)	8.45(0.15)	21.83(0.2)	94.08	0.040
13	$R\bar{3}$ 6*f* ($xyz = \frac{811}{884}$)	9.30(0.1)	8.71(0.2)	5.83(0.1)	8.51(0.15)	21.54(0.2)	92.80	0.039
39		7.51(0.1)	7.17(0.2)	4.77(0.1)	6.94(0.15)	21.29(0.2)	91.98	0.039
4.2 (*3*)	$R\bar{3}c'$ 6*e*	1.12	6.24	6.24	8.90(0.02)	28.07(0.02)	−90.0	0.060
5	$R\bar{3}c'$	3.99(0.1)	7.73(0.2)	9.96(0.1)	8.76(0.15)	34.72(0.2)	−72.43	0.040
13	6*f'* ($xyz = \frac{754}{884}$)	4.33(0.1)	7.33(0.2)	9.93(0.1)	8.54(0.15)	32.85(0.2)	−75.61	0.039
39		4.54(0.1)	7.53(0.2)	7.46(0.1)	7.09(0.15)	23.52(0.2)	−72.65	0.039

Note. Magnetic moments are given in Bohr magnetons (μ_B).

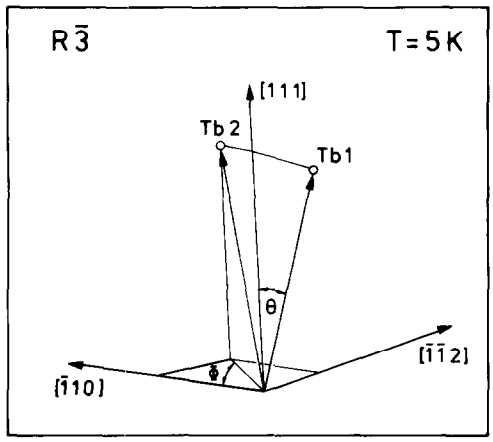

FIG. 4. Spin configuration at 5 K showing spins at sites $6f$ and $6f'$ in $R\bar{3}$ together with the [111], [$\bar{1}$10], [11$\bar{2}$] coordinate system.

The reflection {200} decreases rapidly with increasing temperatures and vanishes above 39 K. The magnetic moments m(Tb1) and m(Tb2) are equal within experimental error at 5 and 13 K.

Discussion

Deformation of the Polyhedra

The polyhedra around the cations are already slightly distorted in the cubic room-temperature structure. The distortion increases with decreasing temperature. In order to magnify this effect we present "deformation polyhedra plots." We calculated the difference vectors of the oxygen positions between 5, 13, and 39 K with the room temperature value expressed by $r_{oxy}(\text{def}) = r_{oxy}(T = 5, 13, 39\ \text{K}) - r_{oxy}(300\ \text{K})$. The vectors are calculated in angstroms, normalized to the corresponding rhombohedral cell length. A plot of these difference vectors yields a polyhedron as a direct visualization of the low-temperature deformation. The calculated difference vectors are of course small with displacements between $0.02\ \text{Å} < r_{oxy}(\text{def}) < 0.1\ \text{Å}$ whereas the mean error of the refined positions is $\Delta(r) = 0.015$ Å.

In Fig. 6a we show the octahedron around the iron atom in the position (0, 0, 0). This atom is located on the threefold axis with site symmetry $\bar{3}$. In addition three deformation polyhedra are plotted (Fig. 6a). They represent the distortion of the oxygen environment of this site. The plots are in angstroms and it is worth noting the different scale of the octahedron and the deformation polyhedra as marked in the figure. The orientation of the polyhedra is indicated by [111] in the plots. The defor-

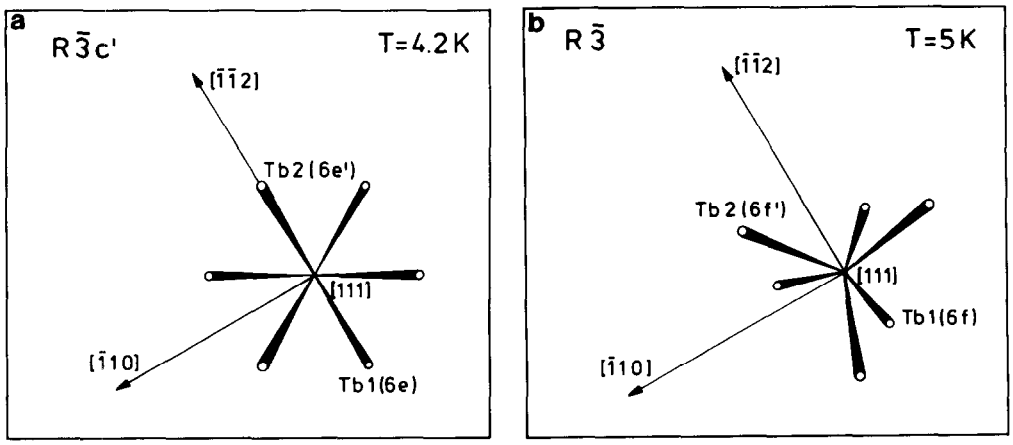

FIG. 5. Comparison of magnetic structures as refined in $R\bar{3}c'$ (3) (a) and $R\bar{3}$ (b) (this work).

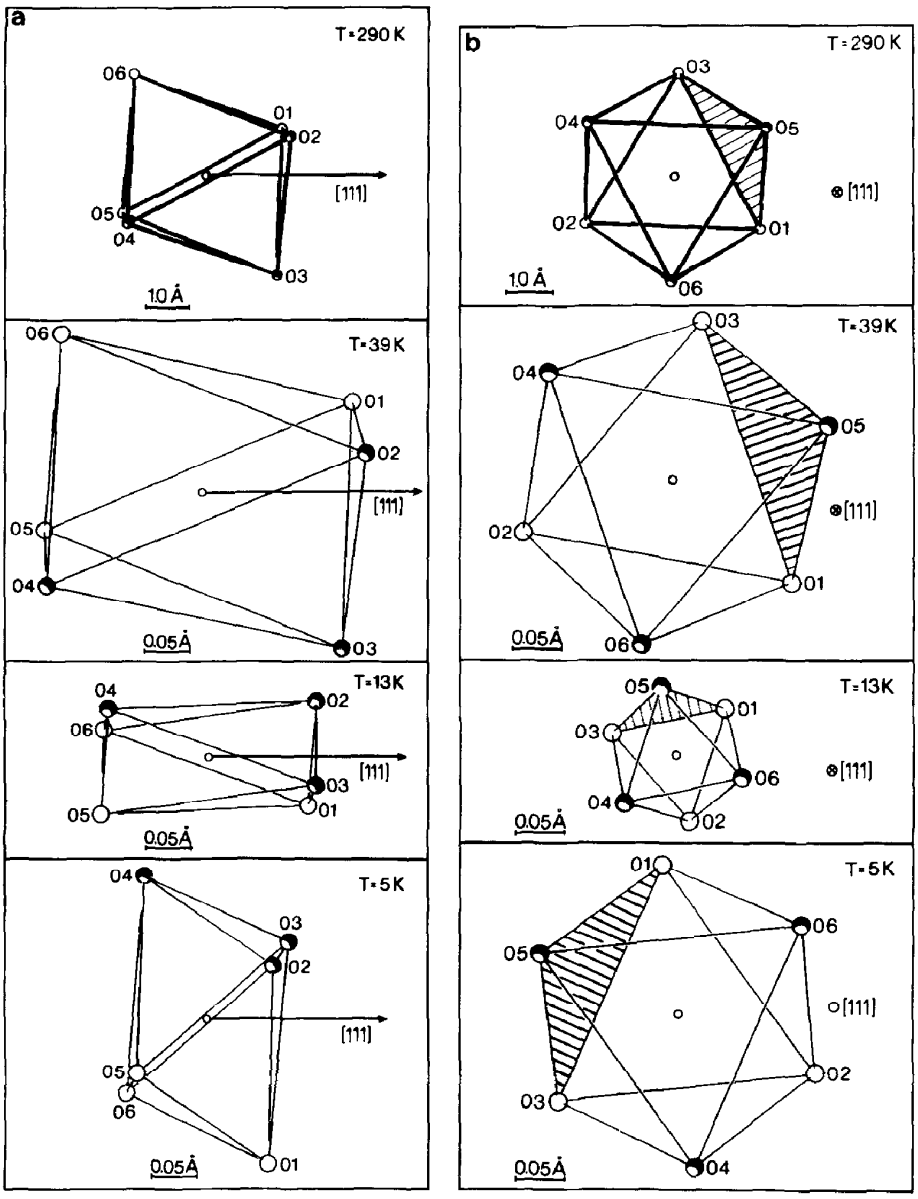

FIG. 6. Oxygen octahedron and corresponding deformation polyhedra around the central iron atom in position (0,0,0).

mations at all temperatures are best described as an antiprism. The volume of the antiprism is decreasing from 39 to 13 K, which means that the octahedron is closer to its room-temperature shape at 13 than at 39 K. Between 13 and 5 K the longest axis of the antiprism changes to an orientation almost orthogonal to the [111] axis and again the overall deformation increases. This result is particularly interesting because already at 13 K the final low-temperature magnetic structure is established and

the change in local deformation cannot be directly correlated to a further change in spin configuration. A rotational component of the deformation is recognized by a projection parallel to [111]. The endpoints of the difference vectors of atoms O(1)–O(5)–O(3) are rotated around the [111] direction. This is clearly seen looking at the shaded face O(1)–O(5)–O(3) of the deformation polyhedra.

Another interesting result is the deformation around a tetrahedrally coordinated iron (position $\frac{5}{8}$, $\frac{3}{8}$, $\frac{1}{4}$ in the rhombohedral system). As pointed out by Novik and Ofer (*20*, *21*) the most important interaction of the Fe–Re exchange is between the rare earth and its two nearest-neighbor tetrahedral Fe sites. If this exchange path is important for the formation of the low-temperature umbrella-like Tb^{3+} spin structure, we expect this fact to be reflected in the local deformation around Tb and its nearest-neighbor Fe sites. A plot of the deformation polyhedron shows (Fig. 7) that the deviation is largest for O(2), which lies on the shortest exchange path between Tb and Fe. The effect is most pronounced at 5 K, but at all temperatures O(2) deviates most from the high-temperature position. Again we mark in all plots the orientation of the tetrahedron and the deformation polyhedra by means of the [111] axis.

As a consequence, if one looks at the deformation around Tb, the oxygen shared with the tetrahedral Fe shows the greatest deviation. In addition to this feature the deformations around the Tb atoms show no pronounced symmetry. This is expected, since the Tb sites are general positions in $R\bar{3}$.

The observed distortions can be rationalized if the garnet structure is described in terms of rod packing, a scheme introduced by O'Keefe and Andersson (*22*). These authors demonstrated that the deviation of the real from the ideal garnet structure (based on a *bcc* rod-packing model) in the cubic

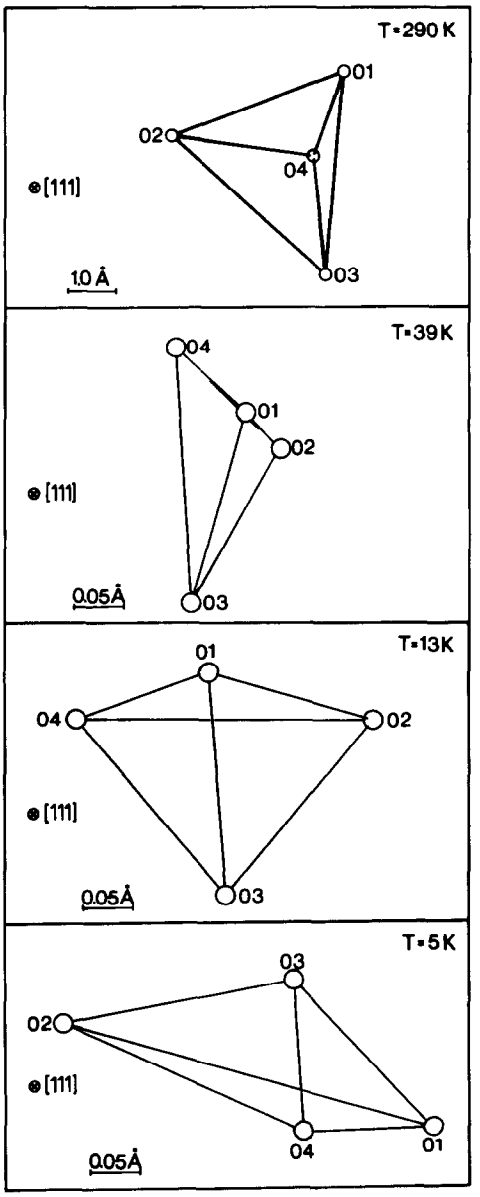

FIG. 7. Oxygen tetrahedron and deformation polyhedra around the central iron atom in position ($\frac{5}{8}$, $\frac{3}{8}$, $\frac{1}{4}$).

system may be explained by three different contributions:

(i) a compression or expansion of the octahedra along the trigonal axis which destroys the regularity of the tetrahedra. Our

difference polyhedra display an expansion between 39 and 5 K.

(ii) a rotation of the octahedra about the trigonal axis.

(iii) an umbrella-like distortion in which the oxygens move in the plane perpendicular to the threefold axis. This distortion is observed between 13 and 5 K.

Bulk Magnetization and Reduced Iron Moments

As mentioned previously the Fe^{3+} moments are considerably reduced compared to the expected free ion value of 5 μ_B at T = 0 K for the $S = \frac{5}{2}$ state of Fe^{3+}. We calculated the magnetization along the three cubic crystallographic directions [111], [110], and [100] to be $M(111) = 37.0\ \mu_B$, $M(110) = 30.21\ \mu_B$, and $M(100) = 21.36\ \mu_B$. These values do not agree well with magnetization measured by Guillot and Le Gall (*23*). They obtained $M(111) = 34.6\ \mu_B$, $M(110) = 28.28\ \mu_B$, and $M(100) = 20.00\ \mu_B$. The differences are mainly due to the contributions of the iron sublattices to the net magnetization. The magnetization per mole (1 mole = 2 formula units of $\{Tb_3\}(Fe_2)[Fe_3]O_{12}$) due to the Tb^{3+} ions gives only minor differences between our results and former work (*23–25*). The refinement yields $M(Tb) = 45.22\ \mu_B$/mole for the total magnetization of the two Tb sublattices and Lahoubi refines a value of $M(Tb) = 44.64\ \mu_B$/mole (*3*). The difference of the two models is $\delta(M) = 0.58\ \mu_B$/mole and is within the range of results for the magnetization as found in the literature.

The question why neutrons probably "see" reduced magnetic moments was discussed recently by Ligenza (*26* and references therein) for the spinel $MnFe_2O_4$ and for yttrium iron garnet. Ligenza states that a decrease in static magnetic moments at the iron sites in YIG is probably due to the appearance of different dynamic magnetic configurations for the ions in a crystallographic site with a certain number of magnetic neighbors. Due to the dynamic nature of superexchange, the unperturbed magnetic ground state of Fe^{3+} $^6S_{5/2}$ is not realized at any time for the ion in an electric crystal and magnetic molecular field. On the contrary, the actual magnetic configuration fluctuates with typical relaxation times between $10^{-8}\ s \gg t \gg 10^{-13}$ s. The neutron interaction time is approximately $t = 10^{-13}$ s. Therefore the neutron may observe distinct magnetic states of the ion in its crystal environment and only with a certain probability the saturated groundstate of 5 μ_B. In fact reduced moments have been observed by polarized neutrons on a YIG single crystal (*8*). Other reasons for reduced moments are covalent bonding (*8*) and topological frustration as discussed for example by Ferey *et al.* for FeF_3 (*19*).

Conclusion

The performed experiment shows that detailed information about the local microscopic deformations around single ions in TbIG can be obtained by neutron powder diffraction. A systematic study over a larger temperature range could yield the evolution of these deformations in correlation with the structural changes in the spin configuration. The concept of plotting deformation polyhedra is shown to be a helpful tool to visualize small deformations in complex structures such as garnets.

Acknowledgments

Support of this work by the Bundesminister für Forschung und Technologie (Bonn, FRG) under Contract 03-Ful-FRAO is gratefully acknowledged. The authors thank M. Guillot for the sample.

References

1. E. F. Bertaut and F. Forrat, *C.R. Seances Acad. Sci.* **242,** 382 (1956).
2. F. Tchéou, H. Fuess, and E. F. Bertaut, *Solid State Commun.* **8,** 1745 (1970).

3. M. LAHOUBI, M. GUILLOT, A. MARCHAND, F. TCHÉOU, AND E. ROUDAUT, *IEEE Trans. Magn.* **20,** 1518 (1984).
4. F. TCHÉOU, Thesis, No. A.O. 7632, University of Grenoble, France (1972).
5. F. SAYETAT, *J. Appl. Phys.* **46,** 3691 (1975).
6. F. SAYETAT, *J. Magn. Magn. Mater.* **58,** 334 (1986).
7. F. SAYETAT, J. X. BOUCHERLE, AND F. TCHÉOU, *J. Magn. Magn. Mater.* **46,** 219 (1984).
8. M. BONNET, A. DELAPALME, H. FUESS, AND P. BECKER, *J. Phys. Chem. Solids* **40,** 863 (1979).
9. J. BARUCHEL, J. P. GUIGAY, C. MAZURE-ESPEJO, M. SCHLENKER, AND J. SCHWEIZER, *J. Phys.* Coll. C7, Tome 43 **C7,** 101 (1982).
10. J. P. GUIGAY, M. SCHLENKER, AND J. BARUCHEL, "Neutron Scattering in Almost Perfect Magnetic Crystals" *in* "Applications of X-Ray Topography Methods to Material Science (S. Weissman, F. Balibar, and J. F. Petroff, Eds.), *Plenum,* New York (1984).
11. A. HEWAT, "D2B, A New High Resolution Neutron Powder Diffractometer At ILL Grenoble" *in* "High Resolution Powder Diffraction" (C. R. A. Catlow, Ed.), *Materials Science Forum,* Vol. 9, p. 69 (1986).
12. H. M. RIETVELD, *J. Appl. Cryst.* **2,** 65 (1969).
13. R. E. WATSON AND A. J. FREEMAN, *Acta Crystallogr.* **14,** 27 (1961).
14. A. J. FREEMAN AND J. P. DESCLAUX, *J. Magn. Magn. Mater.* **12,** 11 (1979).
15. V. F. SEARS, "Thermal Neutron Scattering Lengths and Cross Sections for Condensed Matter Research, AECL-8490, Chalk River Nuclear Laboratories (1984).
16. H. FUESS, G. BASSI, M. BONNET, AND A. DELAPALME, *Solid State Commun.* **18,** 557 (1976).
17. E. F. BERTAUT, *Ann. Phys.* **7,** 203 (1972).
18. G. P. ESPINOSA, *J. Chem. Phys.* **37,** 2344 (1962).
19. G. FEREY, R. DE PAPE, M. LEBLANC, AND J. PANNETIER, *Rev. Chim. Miner.* **23,** 474 (1986).
20. I. NOVIK AND S. OFER, *Phys. Rev.* **153,** 409 (1967).
21. U. ATZMONY, E. R. BAUMINGER, A. MUSTACHI, I. NOVIK, S. OFER, AND M. TASSA, *Phys. Rev.* **159,** 514 (1969).
22. M. O'KEEFE AND S. ANDERSSON, *Acta Crystallogr. A* **33,** 914 (1977).
23. M. GUILLOT AND H. LE GALL, *J. Phys.* **7,** 38–871 (1977).
24. S. GELLER, H. J. WILLIAMS, R. C. SHERWOOD, J. P. REMEIKA, AND G. P. ESPINOSA, *Phys. Rev.* **137,** 1034 (1965).
25. S. D. GELLER, H. J. WILLIAMS, R. C. SHERWOOD, J. P. REMEIKA, AND G. P. ESPINOSA, *Phys. Rev.* **131,** 1080 (1963).
26. S. LIGENZA, *Phys. Status Solidi B* **131,** 105 (1985).